Photocatalytic activity of TiO2/stevensite nanocomposites for the removal of Orange G from aqueous solutions

Lahcen Bouna, Benaïss Rhouta, Francis Maury, Amane Jada, François Senocq, Marie-Christine Lafont

Photocatalytic activity of TiO_2/stevensite nanocomposites for the removal of Orange G from aqueous solutions

L. BOUNA[1], B. RHOUTA[1], F. MAURY[2], A. JADA[3,*], F. SENOCQ[2] AND M.-C. LAFONT[2]

[1] *Laboratoire de Matière Condensée et Nanostructures (LMCN), Faculté des Sciences et Techniques Guéliz, BP 549, Marrakech, Morocco,* [2] *CIRIMAT, ENSIACET, 4 Allée Emile Monso, BP 44362, 31030 Toulouse Cedex 4, France, and* [3] *IS2M, 15 rue Jean Starcky BP 2488, 68057 Mulhouse Cedex, France*

ABSTRACT: TiO_2/stevensite nanocomposite photocatalysts were synthesized by a solvothermal method using $TiCl_3$/HCl as reactants and the stevensite clay mineral extract as support. The prepared photocatalyst samples were then characterized using various techniques such as X-ray diffraction (XRD), Infrared spectroscopy (IR) and Transmission Electron Microscopy (TEM). The Points of Zero Charge (PZC) of the various samples were evaluated by titration of the non-modified and the Ti-modified clay aqueous dispersions, with cationic surfactant solutions. The photocatalytic activity of the resulting nanocomposites samples were evaluated for the removal of Orange G (OG) from aqueous solution as a model dye pollutant. The data indicate that the formation of Na^+-stevensite by the TiO_2 particles leads to TiO_2/stevensite nanocomposites having higher specific surface areas and mesopore volumes, and lower PZC values. Further, the photocatalytic activity was found to be greater for the TiO_2/stevensite nanocomposites having the greatest Ti amount, as compared to a pure TiO_2 sample, and increased with the increase of the TiO_2 amount in the TiO_2/stevensite nanocomposites.

KEYWORDS: clay, titanium dioxide, stevensite, photocatalysis, streaming induced potential, nanocomposites.

In recent years, several studies and methods have been carried out to achieve the removal of organic pollutants present in waste water. One of these methods has concerned the adsorption and degradation of organic dye by using TiO_2 particles supported on clay minerals as a nanocomposite photocatalyst (Hadnadjev-Kostic *et al.*, 2013; Henych & Štengl, 2013). Moreover, the use of organo- or inorgano-modified clay or clay-based nanocomposite materials is an emerging area of nano-technology which may be applied to environmental remediation strategies (Seung Mok & Diwakar, 2012). Thus, pillaring clay surfaces with a Ti precursor (Ti-PILC) leads after calcinations of the samples at 500ºC to photocatalytic active materials (Khalfallah Boudali *et al*., 1994; Feng *et al*., 2003; Houari *et al.*, 2005; An *et al*., 2008).

Furthermore, among the methods used to prepare nanocomposite photocatalysts, the sol-gel route, called also 'the colloidal method' was first proposed by Aranda *et al.* (2008) to promote the spontaneous formation of a gel from a sol of a Ti precursor/alcohol in the presence of an alcoholic dispersion of sepiolite. Thus, the term 'colloidal method' used in the literature (Bouna *et al.*, 2011) implies a sol-gel route in which colloids corresponding to clay minerals are involved. Here, to

* E-mail: amane.jada@uha.fr
DOI:

avoid any ambiguity, the term 'colloidal method' is replaced by sol-gel. Hence, according to Aranda *et al*. (2008), the sol-gel route leads to the immobilization of the TiO_2 particles onto the clay surface. However, the best photocatalytic activity of the resulting composite material was obtained only after calcination of the sample at 600ºC (Aranda *et al*., 2008; Bouna *et al*., 2011). Others photocatalyst nanocomposites formed from titania-pillared montmorillonite were prepared by a solvothermal reaction using water and ethanol as solvents, hexamethylenetetramine as precipitant, and titanium trichloride as precursor (Liu *et al*., 2009). In this case anatase (TiO_2) was obtained at a sample temperature treatment of only 190ºC inside an autoclave, and without further calcinations. A variety of clay minerals, either natural or synthetic, has been used as supports for preparing the photocatalyst nanocomposites, namely montmorillonite (Khalfallah Boudali *et al*., 1994; An *et al*., 2008; Liu *et al*., 2009), saponite (Ooka *et al*., 2004; Nikolopoulou *et al.*, 2009), laponite (Paul *et al*., 2012), sepiolite (Aranda *et al*., 2008), ferruginous beidellite-rich clay (Bouna *et al*., 2012b) and palygorskite fibrous clay (Bouna *et al*., 2011).

We have recently undertaken a general research program aimed at developing innovative clay-based materials starting from low-cost natural clay. Thus, we first identified several Moroccan clay deposits that we characterized along with their fine fractions (<2 μm) (Bouna *et al*., 2012b; Rhouta *et al*., 2008, 2013) before considering them in various applications as adsorbent (Bouna *et al*., 2010), as photocatalysts supports (Bouna *et al*., 2011, 2012a, 2013) or as micro containers of metallic corrosion inhibitors (Aït Aghzzaf *et al*., 2012, 2014). The Rhassoul clay, made up of ~95% of stevensite and ~5% of carbonate (Rhouta *et al*., 2008), comes from a commercial Moroccan deposit, located to the east of the Middle Atlas Mountains, in the Moulouya Valley, ~200 km from Fes and exploited for the export market by the Sefrioui group of the Rhassoul company and its derivatives (Rhouta *et al*., 2008; Benhammou *et al*., 2009). The Rhassoul clay has been used for several centuries in natural cosmetic products (soap, shampoo, skin conditioner) and, besides cosmetic purposes, it is now marketed for its detergent and grease-removing properties. All these virtues are due to the stevensite contained in the Rhassoul clay. As a trioctahedral Mg-rich smectite, the stevensite can thus be easily modified to yield advanced innovative materials for numerous applications.

In the present work, stevensite isolated from natural Moroccan Rhassoul clay (Rhouta *et al*., 2008; Bouna *et al*., 2010) has been modified by using a solvo-thermal method (Liu *et al*., 2009) to obtain TiO_2/stevensite nanocomposites. Carrying out a general program aimed at assessing Moroccan natural clays, the synthesis of TiO_2/stevensite was undertaken to investigate the potential of these nanocomposite materials as new supported photocatalysts. Both these environmentally friendly materials and the low cost of the solvo-thermal process used for their synthesis make these photocatalytic materials attractive for the industrial removal of pollutants from waste water. The photocatalytic activity of the resulting nanocomposite samples was tested for the removal of OG (Orange G, a dye widely used in textile industry) from aqueous solutions. This organic azo dye compound, namely 1-phenylazo-2-naphthol-6,8-disulfonic acid disodium salt, was selected as the model pollutant. It is frequently used as a reagent in the photocatalytic tests either under visible or UV irradiation. Here this anionic dye compound was selected as the model pollutant because we previously demonstrated that its adsorption onto clay minerals was negligible due to electrostatic repulsion between the negatively charged clay particles and the anionic dye (Bouna *et al.*, 2010). The photocatalytic activity data are discussed in relation to the specific structural features of the material and are then compared to that of a pure TiO_2 sample.

MATERIALS AND METHODS

Materials

The Orange G, (CAS number 1936-15-8, molecular weight = 452.38 g mol^{-1}, pKa = 11.5) was purchased from Aldrich, and used as received without further purification. The natural clay (stevensite) was the same as used elsewhere (Bouna *et al.*, 2010). The titanium precursor $TiCl_3$ used as pillaring agent was purchased from Aldrich.

Obtaining the stevensite fine fraction from the raw Rhassoul clay

After being crushed and sieved through a 50 μm filter, an aqueous dispersion of a given mass of raw

Rhassoul clay was first reacted with hydrochloric solution (2 M) at pH = 4 to remove carbonate impurities. The dispersion was then centrifuged and the solid washed several times until the supernatant pH reached 7. Thereafter, the stevensite-rich fine fraction (particle size <2 μm), was separated from the 5 wt.% clay dispersion according to Stokes' law (Holtzapffel, 1985). This operation was repeated several times until the dispersion was almost transparent. The fine fraction was recovered by centrifugation at 3500 rpm for 40 min and then treated, by stirring for 12 h with NaCl solution (1 M) in order to saturate the interlayer spaces of stevensite with Na^+ ions. This operation was repeated four times to ensure complete exchange of the interlayer cations by Na^+. Homoionic sodium stevensite (designated Na^+-stevensite) was recovered by repetitive washing with distilled water until free of chloride, as confirmed by the $AgNO_3$ test. Na^+-stevensite was finally dried at 353 K. As previously reported (Rhouta *et al*., 2008; Bouna *et al*., 2010), the cationic exchange capacity (CEC), the BET specific surface area and total pore volume of the stevensite from Jbel Rhassoul were assessed to be around 60 meq/100g, 150 m^2/g and 0.039 cm^3/g respectively. Its structural formula was determined to be $(Na_{0.25}K_{0.20})(Mg_{5.04}Al_{0.37}Fe_{0.20}\square_{0.21})_{5.61}(Si_{7.76}Al_{0.24})_8O_{20}(OH)_4$.

Preparation of TiO_2/stevensite nanocomposites

A quantity of Na^+-stevensite powder was dispersed in a solvent mixture consisting of 50 mL of distilled water and 50 mL of ethanol. The resulting dispersion was stirred vigorously for 1 h before use. The pillaring agent was prepared by adding an aqueous solution containing 20 wt.% of $TiCl_3$ to an ethanol solution to yield a final solution having a Ti^{3+} concentration of 0.8 M, by using a similar procedure as described elsewhere (Liu *et al*., 2009). This Ti^{3+} final solution was then added to a water/ethanol stevensite dispersion at the desired $TiCl_3$/stevensite mass ratios, and the resulting inorgano-clay mixture allowed to react for 4 h at room temperature under stirring. Finally a desired amount of hexamethylene tetramine (HMT), used as a precipitant, was added at a fixed ratio of 8 mol $TiCl_3$ per mol HMT, and the resulting mixture was heated in a 200 mL stainless-steel autoclave at 190ºC for 3 h. At the end of the reaction, the sample was cooled naturally to room temperature, then centrifuged, washed several times with distilled water and ethanol to make sure that Cl^- was absent (checked by $AgNO_3$ solution), and vacuum dried at 60ºC for 24 h. It should be noted that by varying the $TiCl_3$/stevensite mass ratios, it was possible to prepare two samples having $m(TiO_2)$:m(stevensite) = 0.2:1 and 0.4:1 (which are referred to as Ti-stev-0.2 and Ti-stev-0.4, respectively).

Characterization methods

The purified natural Rhassoul (Na^+-stevensite) sample was characterized before and after its treatment by TiO_2. X-ray diffraction (XRD) data were recorded at room temperature over the same angular range using a Seifert XRD 3000TT diffractometer equipped with a graphite monochromator (Bragg-Brentano configuration; Cu-$K\alpha$ radiation). The specific surface areas of the dried samples were determined using the Brunauer–Emmett–Teller (BET) method (Brunauer *et al*., 1938); nitrogen adsorption isotherms at 77 K were utilised using an adsorption analyser from Micromeritics (ASAP 2020 V 3.01 H). Prior to the N_2 adsorption-desorption measurements, the samples weighing 150 mg were out-gassed at 150ºC for 24 h. Infrared (IR) spectroscopic studies were undertaken using a Nicolet apparatus under ambient conditions over the frequency range 400−4000 cm^{-1} using KBr pellets. The pellets were obtained by pressing a mixture of 2 mg of clay material with 198 mg of KBr (~1 wt.%). Microstructural observations were performed with a JEOL JEM 2010 Transmission Electron Microscope (TEM) equipped with TRACOR EDS software also enabling local elemental compositions to be obtained. The Ti compositions of the various samples were determined after total fusion, by induced coupled plasma spectrometry (ICP) using Series X2 equipment from Thermo Electron, equipped with a Meinhard nebuliser and an ETP simulscan detector. ^{47}Ti and ^{49}Ti isotopes were used with collision cell technology.

In order to investigate the effect of the clay modification by Ti on the electrical properties of the clay aqueous dispersions, the Points of Zero Charge (PZC) of the various samples were evaluated by titration of the stevensite, pure TiO_2, or the TiO_2/stevensite nanocomposite aqueous dispersions, with a cationic surfactant (cetyltrimethylammonium chloride, CTAC). This surfactant was selected as the titrant from various samples

for two main reasons. The first one is due to the adsorptive properties of the CTAC molecules which may adsorb on hydrophilic, as well as, on hydrophobic surface sites. The second reason is based on the well known surface characteristics of the CTAC molecules in water, such as the head group surface area per CTAC molecule, σ = 58.63 Å^2 (Jada *et al*., 2006). The streaming induced potential (SIP) of various samples were measured for each addition of a known CTAC amount to a known amount of the sample dispersed in water. An electrical potential device (Particle Charge Detection, PCD, Müteck Instruments) was used to measure the SIP, as described elsewhere (Jada *et al*., 2006; Bouna *et al*., 2010).

Photocatalytic activity

The photocatalytic activities of different samples were evaluated by measuring the decomposition rate of OG aqueous dispersions containing the photocatalyst (TiO_2 or TiO_2/stevensite nanocomposite). The degradation reaction was carried out in a batch quartz reactor (40 mm × 20 mm × 36 mm) placed in a thermostat chamber (25ºC) under UV light (HPLN Philips 125 W) emitted at 365 nm. The reactor was irradiated with a photon flux of 1 mW.cm^{-2} by adjusting the distance to the lamp which emitted radiations resembling the emitted UV intensity of solar spectrum on the earth surface (Hofstadler *et al*., 1994). The photocatalyst powder was dispersed in 25 cm^3 of OG solution (10^{-5} m) to yield a final concentration equal to 1 g dm^{-3}, and then the mixture was stirred with an inert Teflon magnetic stirrer. To determine the residual dye concentration, aliquots were taken from the mixture of the dye-photocatalyst dispersion, at regular time intervals and centrifuged at 11062 × g. The OG concentration in the supernatant was then determined by measuring the absorbance at 480 nm using a UV-VIS-NIR spectrophotometer (Perking Elmer lambda 19).

RESULTS AND DISCUSSION

X-ray diffraction

Figure 1 shows the X-ray powder patterns of natural Na^+-stevensite clay, before and after its modification by Ti (Ti-stev-0.4). As can be seen in the figure, the Na^+-stevensite clay displays a very weak reflection peak at 2θ = 26.6º corresponding to quartz impurities and shows the characteristic peaks of the mineral stevensite at 2θ = 5.74º (d_{001} = 15.2 Å), corresponding to the very intense basal reflexion (001) and the less intense harmonic (002) reflexion at 2θ = 12.46º (d_{002} = 7.09 Å) and (003) peak at 2θ = 17.81º (d_{003} = 4.97 Å). The observation of these harmonics in addition to the principal reflexion probably denotes the relative good crystal-

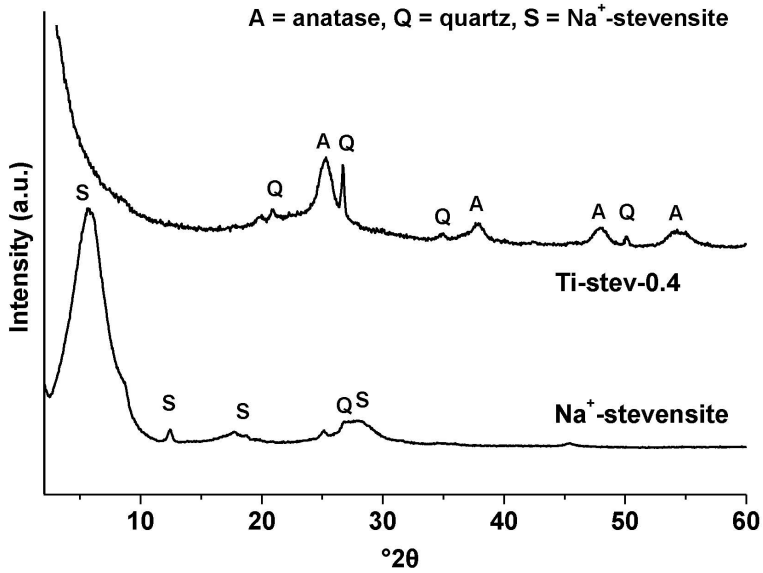

FIG. 1. X-ray diffraction patterns of Na^+-stevensite and modified nanocomposite (Ti-stev-0.4).

linity of the stevensite investigated. In addition, Fig. 1 indicates that the TiO_2-modified Na^+-stevensite does not show any characteristic peaks of the phyllosilicate, and the peaks observed at $2\theta = 25.2^o$, 37.8^o, 48^o and 54.3^o are attributed to an anatase phase (TiO_2) phase that has been formed after formation of Na^+-stevensite by the solvothermal method. This result seems to indicate that the damage to the clay mineral layers by the preparation procedure results in the loss of stacking order (i.e. the absence of an XRD peak at low angles). Nevertheless, the absence of basal reflexion of saponite was also observed by Nikolopoulou *et al.* (2009) in a saponite-TiO_2 nanocomposite prepared by the same solvothermal procedure, particularly for a TiO_2:saponite mass ratio around 0.2.

Our results are also in agreement with previously reported work (An *et al*., 2008), where a decrease and/or an absence of the (001) basal reflection of the clay mineral was observed with an increasing amount of TiO_2 in the TiO_2/montmorillonite nanocomposites. According to these authors, this observation is due to either to the formation of large TiO_2 crystals in silicate inter-layer spaces, preventing the existence of parallel layers, and/or to the complete coverage of pillared silicate by TiO_2 particles, instead of the damage to the phyllosilicate. Indeed, a decrease of the clay mineral XRD peaks is expected due to the screening effect of TiO_2 grown on clay mineral supports. In this respect, Bouna *et al.* (2011) reported that the basal reflection peak intensity decreased, resulting from the transformation of the amorphous TiO_2 to crystalline TiO_2 anatase, after annealing the TiO_2/palygorskite nanocomposites. On the other hand, Fig. 1 also indicates that the peak at $2\theta = 26.6^o$, corresponding to quartz, increases in intensity. The sharp shape of this peak denotes that the silica is crystalline so that the peak intensity increase cannot be ascribed to the transformation of the stevensite into silica under solvothermal procedure conditions. Indeed, the clay mineral transformation, well known to occur under severe acid conditions, yields amorphous silica (Frini-Srasra & Srasra, 2010). Thus, the increase of the peak intensity of quartz in the TiO_2-stevensite nanocomposite is likely to be due to the remaining quartz impurity which, under solvothermal conditions, became free from stevensite particles that embedded the quartz in the starting clay mineral.

Infrared spectroscopy

The infrared spectra of the Na^+-stevensite and the TiO_2/stevensite nanocomposites, obtained by using the two TiO_2/stevensite mass ratios 0.2:1 and 0.4:1, are shown in Fig. 2. The infrared spectrum of the

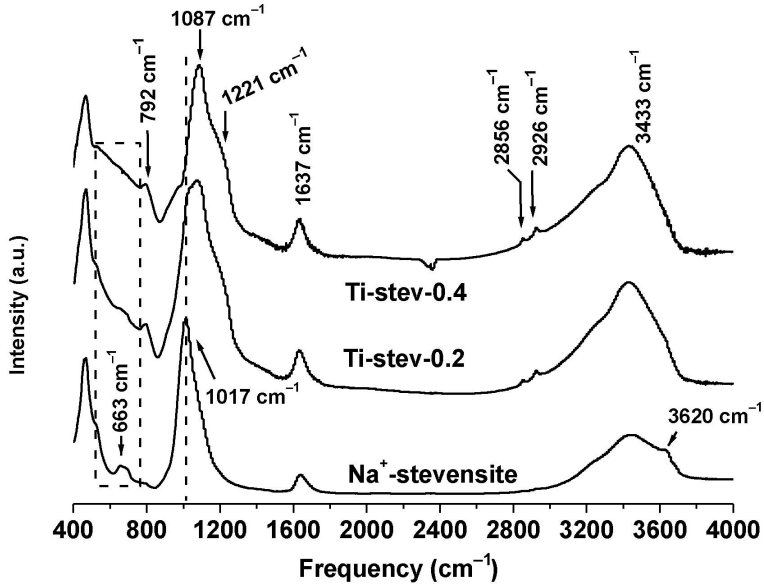

FIG. 2. Infra-red spectra of Na^+-stevensite, and modified nanocomposite samples (Ti-stev-0.2 and Ti-stev-0.4).

non-modified Na^+-stevensite is similar to that described in detail elsewhere (Rhouta *et al*., 2008). Hence, the absorption peak at about 1017 cm^{-1} corresponds to Si−O stretching vibration of the tetrahedral layer, whereas the absorption peak at 3621 cm^{-1} is attributed to the silanol (SiOH) clay surface groups. Figure 2 shows that the samples Ti-stev-0.2 and Ti-stev-0.4 exhibit additional vibration bands at 792 and a shoulder at 1221 cm^{-1}, which are not present in Na^+-stevensite. These new peaks are ascribed to quartz, in agreement with the above XRD analysis. In addition, Fig. 2 also shows that the infrared spectra of the TiO_2-modified clay samples display peaks at 2856 cm^{-1} and 2926 cm^{-1} (C−H stretching mode) with low intensities. Such peaks are attributed to residual organic species such as (Hexamethylene tetramine) used as precipitant (see section dealing with the preparation of TiO_2/stevensite nanocomposites). Furthermore, in Fig. 2, the intense peak at 1017 cm^{-1} occurring in Na^+-stevensite is shifted to a higher frequency, around 1087 cm^{-1} in the TiO_2-modified clay samples. The occurrence of this shift results from the formation of bonding between $(SiO_4)^{4-}$ and TiO_2, and indicates a small distortion in the symmetry of the tetrahedral sheets. Further, an increase in the Si−O band frequency, resulting from an increase in the heterogeneous bonding of Ti−O−Si in the framework, weakens the Si−O bonding strength (Paul *et al*., 2012). It should be noted that subsequent to the interaction occurring between the clay surface silanol groups with the TiO_2 nanoparticles, the band associated with these groups at 3620 cm^{-1} disappears as depicted in Fig. 2. Finally, the infrared data indicate that the bands occurring at 1637 cm^{-1} and 3433 cm^{-1}, which are attributed to physisorbed water vibrations, are very intense in the TiO_2/stevensite nanocomposites compared with the non-modified clay.

Microstructure characterization

TEM images of the Na^+-stevensite sample and modified clay photocatalyst (Ti-stev-0.4) are presented in Fig. 3a and b, respectively. Figure 3a shows that the Na^+-stevensite sample is organized in the form of stacked sheets having a spacing of ~1 nm, which is characteristic of the smectite family. However, Fig. 3b indicates that the photocatalyst nanocomposite (Ti-stev-0.4) consists of uniform TiO_2 grains embedding stevensite particles as shown by EDS (Energy Dispersive Spectrometry) analysis,

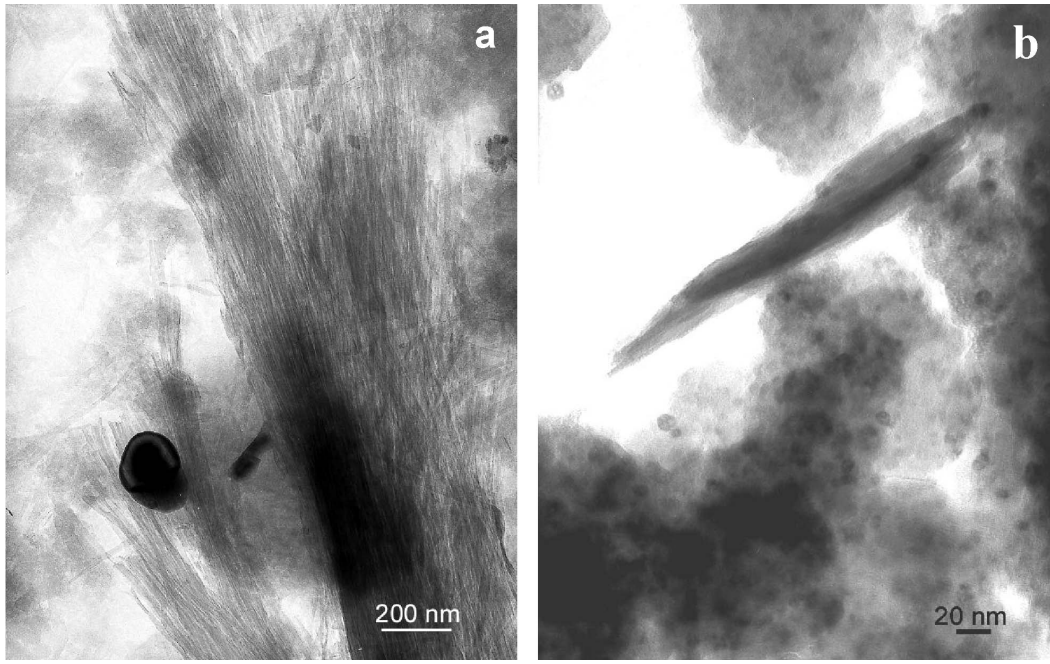

FIG. 3. Transmission electron microscope images showing morphology of Na^+-stevensite and modified nanocomposite (Ti-stev-0.4), images a and b, respectively.

indicating that the elements Si, Al and Mg are contained in the phyllosilicate along with Ti. This further supports the conclusion that the absence of the (001) basal reflexion in the XRD diagram of TiO_2-pillared stevensite (Fig. 1) might be due to the screening effect exerted by TiO_2 particles. Similar data were obtained by Liu *et al.* (2009) in their studies of TiO_2/montmorillonite nanocomposites carried out by the solvothermal method, by Bouna *et al.* (2011) for their investigations dealing with TiO_2/palygorskite-supported photocatalyst prepared by the sol-gel method, and recently by Paul *et al.* (2012) for their synthesis of TiO_2/laponite nanocomposites using a hydrophobic method.

Nitrogen adsorption isotherms

Figures 4, 5 and 6 show respectively, adsorption-desorption isotherms of nitrogen, mesopore size distribution as obtained by BJH method, and micropore size distribution as obtained by Dubinin-Astakhov method, for both the Na^+-stevensite and the synthesized photocatalyst nanocomposites (Ti-stev-0.2 and Ti-stev-0.4). The adsorption-desorption isotherms of nitrogen (Fig. 4) on the Na^+-stevensite surface correspond to type IV with a hysteresis of type H4 according to the IUPAC classification. However, the adsorption-desorption isotherms obtained with the synthesized samples are of type mixed I + II, with a hysteresis of type H3 according to the IUPAC classification. The shape of the isotherms as shown in Fig. 4 indicates that all the samples are mainly mesoporous, but they have also some micropores, resulting from the sharp increase in the adsorbed nitrogen amount at low pressure (Fig. 4). The BET specific surface area (S_{BET}) was determined from these isotherms, by applying BET equation for the relative pressure range $0.02<P/P_0<0.30$. The S_{BET} values determined according to the BET method are, 150, 340, 416 and 68 $m^2\ g^{-1}$ (Table 1) for, respectively, Na^+-stevensite, Ti-stev-0.2, Ti-stev-0.4 and the TiO_2 samples. The two- and about three-fold increases in the surface area resulting from the formation of the Na^+-stevensite are similar to those of TiO_2-clay nanocomposites reported elsewhere by Bouna *et al.* (2011) and Liu *et al.* (2009). Generally, the specific surface area values obtained for TiO_2/clay nanocomposites are higher than those of the starting clay. Therefore, the formation of the clay by TiO_2 allows the preparation of nanocomposites having higher specific surface areas and immobilization of TiO_2 particles on the stevensite surface.

Regarding the sample pore size distributions, Fig. 5 shows the mesopore size distribution curves calculated by the BJH method for the Na^+-stevensite and the modified nanocomposite samples (Ti-stev-0.2 and Ti-stev-0.4). As can be seen, the modification of

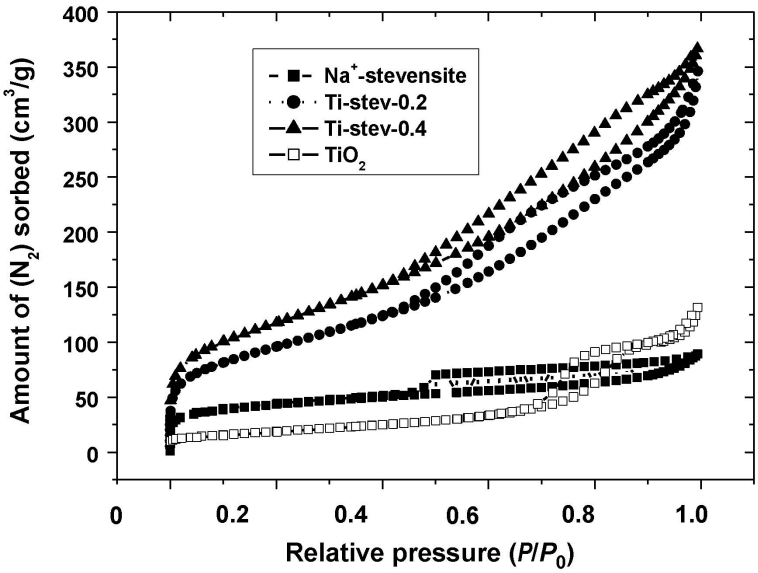

FIG. 4. Nitrogen adsorption-desorption isotherms of the Na^+-stevensite, the TiO_2 prepared in the absence of the clay, and the modified nanocomposite samples (Ti-stev-0.2 and Ti-stev-0.4).

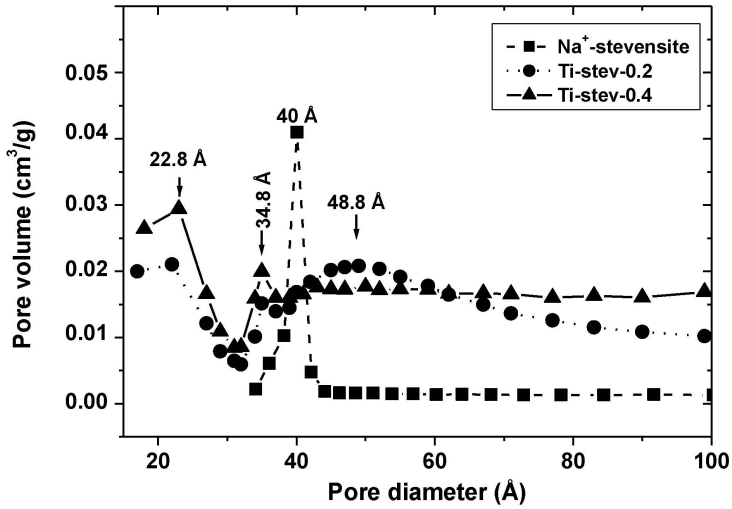

FIG. 5. Mesopore size distribution curves found by the BJH method of Na^+-stevensite and modified nanocomposite samples (Ti-stev-0.2 and Ti-stev-0.4).

the Na^+-stevensite, by TiO_2 particles grown on the clay mineral support leads to the modification of the pore size distributions and it can be discussed in terms of pore filling, pore blocking and pore broadening. As shown in Fig. 5, Na^+-stevensite gives a narrow mesopore size distribution with a mean pore size around 40 Å, whereas samples Ti-stev-0.2 and Ti-stev-0.4 give heterogeneous mesopore size distributions having mean pore sizes below and above 40 Å. Figure 6 shows broad micropore size distributions for the various samples with roughly the same mean micropore size. It can be clearly deduced from the data shown that the modification of the Na^+-stevensite by the TiO_2 particles grown on the clay support does not change the micropore size distribution of the sample. For various samples, the total pore volumes (V_T) were determined from the BJH adsorption cumulative pore volume of pores having diameters in the range 17.0−300.0 nm, whereas the micropore volumes (V_{mic}), the mesopore volumes (V_{mes}) and the external surface areas (S_{ext}) were determined from

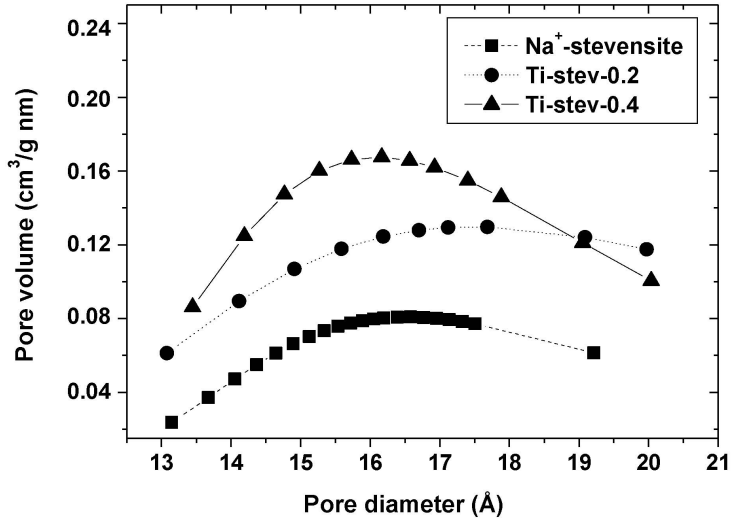

FIG. 6. Micropore size distribution curves found by the Dubinin-Astakhov method of Na^+-stevensite and modified nanocomposite samples (Ti-stev-0.2 and Ti-stev-0.4).

TABLE 1. Specific surface area (S_{BET}), total pore volume (V_T), microporous volume (V_{mic}), mesoporous volume (V_{mes}), micropores surface area (S_{mic}), and external surface area (S_{ext}).

Sample	[a] S_{BET} (m^2 g)	[b] V_T (cm^3/g)	[c] V_{mic} (cm^3/g)	[c] V_{mes} (cm^3/g)	S_{mic} (m^2.g)	[c] S_{ext} (m^2.g)
Na^+-stevensite	150	0.039	0.010	0.028	17	134
[d] TiO_2	68	0.166	0.003	0.091	9	60
Ti-stev-0.2	340	0.254	0.005	0.210	13	328
Ti-stev-0.4	416	0.246	0.014	0.227	31	386

[a] S_{BET} determined by out-gassing the sample at 150ºC for 24 h. [b] Determined from BJH adsorption cumulative pore volume data for pores having diameters in the range 1.7−3 .0 nm. [c] Determined from the *t*-curve (adsorbed volume, V_{ads}. *vs.* the thickness *t*). [d] TiO_2 sample prepared under conditions similar to TiO_2-stevensite nanocomposites in the absence of the clay.

the *t*-curve (adsorbed nitrogen volume, V_{ads}, *vs*. the adsorbed thickness, namely *t*). The microporous surface area (S_{mic}) of each sample was calculated from the difference between the BET surface area (S_{BET}) and the external surface area (S_{ext}). The overall results gathered in Table 1 show that the total pore volume (V_T) and the mesopore volume (V_{mes}) increase with increasing TiO_2 amounts in the TiO_2/stevensite nanocomposites.

Streaming induced potential

The titration of the Na^+-stevensite or the TiO_2/stevensite nanocomposites by cationic surfactant CTAC were carried out by measuring the streaming induced potential (SIP) of the resulting mixture (Jada *et al*., 2006). Thus, upon addition of a given CTAC aqueous solution volume to the aqueous dispersions of Na^+-stevensite or of the synthesized nanocomposite photocatalysts (Ti-stev-0.2 and Ti-stev-0.4), the SIP value was measured. The data are presented in Fig. 7. For the Na^+-stevensite sample, the starting negative surface charges of a given clay mineral amount (20 mg) were compensated progressively with increases in the CTAC amount up to the Point of Zero Charge (PZC) occurring at a CTAC concentration of about 7.7×10^{-6} m. However, the Ti-stev-0.2 nanocomposite shows a

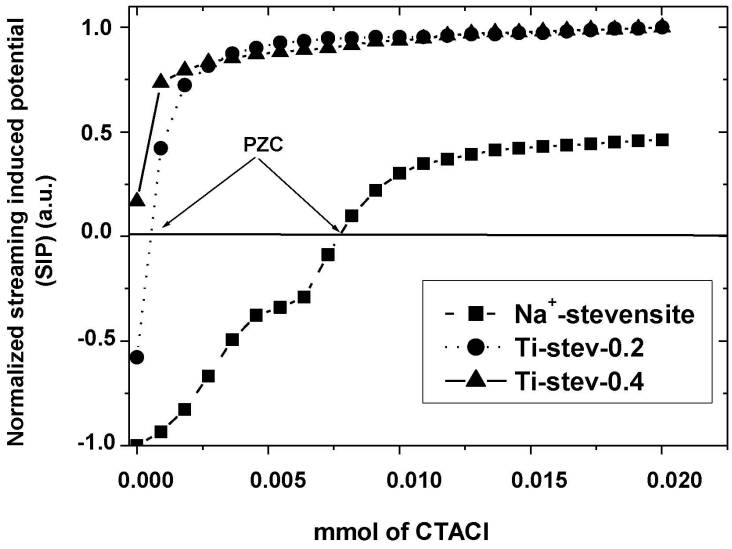

FIG. 7. Variation of normalized Streaming Induced Potential (SIP) curves with a CTAC cationic surfactant added to the aqueous dispersions of Na^+-stevensite, and modified nanocomposite samples (Ti-stev-0.2 and Ti-stev-0.4).

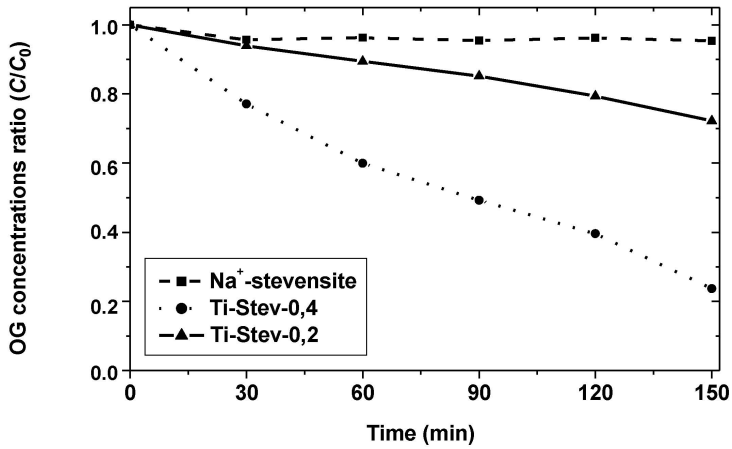

FIG. 8. Photocatalytic degradation curves of Na^+-stevensite, and modified nanocomposite samples (Ti-stev-0.2 and Ti-stev-0.4).

low PZC value of CTAC, occurring at a CTAC concentration an order of magnitude lower, about 5.10^{-7} m. In addition, Fig 7 indicates that the Ti-stev-0.4 nanocomposite has the lowest PZC value. Therefore, the SIP data show clearly a decrease in the PZC value and/or the negative electrical surface charge of the nanocomposite with the increase of TiO_2 amount incorporated in the synthesized sample. It should be noted that no PZC value was observed when the pure TiO_2 sample prepared in the absence on Na^+-stevensite was titrated with CTAC. The pure TiO_2 sample was found to be positively charged before any addition of CTAC.

Photocatalytic activity

Figure 8 shows the degradation rate of Na^+-stevensite and prepared nanocomposite photocatalysts (Ti-stev-0.2 and Ti-stev-0.4) for the removal of OG dye from aqueous solution. According to the blank test, the Na^+-stevensite clay mineral does not exhibit any activity to reduce the OG concentration. This means that, as expected, there is no photocatalytic activity of the Na^+-stevensite alone. However, the synthesized sample Ti-stev-0.2 exhibits a low photocatalytic activity with only about 6% and 20% of OG removed after 30 and 150 min, respectively (Fig. 8 and Table 2). Further, sample Ti-stev-0.4 is more active than the previous one since it has removed 22% and almost 80% of OG in 30 and 150 min, respectively (Fig. 8 and Table 2). The low removal of the dye from the aqueous solution by the Ti-stev-0.2 as compared to Ti-stev-0.4 is due to the low mass of TiO_2 and a relatively low surface area of the Ti-modified clay sample. These two parameters (amount of the TiO_2

TABLE 2. Chemical composition of Ti, degradation and normalized conversion of OG, after 30 min of UV irradiation.

Sample	[a]Ti content (g/100 cm^3 of sample solution)	[b]Degradation of OG (wt.%)	Normalized conversion of OG (wt.% of degraded OG)/ (concentration of Ti)
[c]TiO_2	86.5	92	4.3
Ti-stev-0.2	9.4	6	2.5
Ti-stev-0.4	16.5	22	5.3

[a] Amount of Ti, in the Ti modified clay, as determined by ICP analysis. [b] The degraded OG amount was calculated by using equation $(1 - C/C_0)$, where C_0 ($C_0 = 10^{-5}$ m) and C are the OG concentrations, respectively, before and after 30 min of the UV irradiation. [c] Pure TiO_2 sample prepared under conditions similar to TiO_2-stevensite nanocomposites in the absence of the clay.

and the specific surface area) of the Ti-modified clay are expected to play a major role on the efficiency of photocatalytic activity. Generally, the catalytic activity of pillaring/TiO_2 photocatalysts increases with increasing both the pores volume and specific surface area (Liu *et al*., 2009). In the present work, the two nanocomposite samples, Ti-stev-0.2 and Ti-stev-0.4, were found to have, within an experimental error of ± 1.5%, roughly the same total pore volume V_T. However, the two nanocomposite samples have V_T and S_{BET} values, respectively, 6-times and 3-times greater than the V_T and S_{BET} values of the Na^+-stevensite. Therefore, it can be concluded that both the specific surface area and the total pore volume, V_T, are the key parameters in the catalytic activity of pillaring/TiO_2 photocatalysts.

As can be seen in Table 2, the OG conversion after 30 min has been normalized to the weight of TiO_2 in the sample. This normalization was done in order to neutralize the effect of the TiO_2 amount, and to estimate the effects of the sample specific surface area, S_{BET}, and the total pore volume, V_T. The data reported in Table 2 indicate that the sample Ti-stev-0.4 is the most efficient. The improvement in the photocatalytic activity of the TiO_2/stevensite nanocomposites as compared to Na^+-stevensite results not only from the increase of the sample specific surface area from 150 m^2/g (Na^+-stevensite) to 416 m^2/g (Ti-stev-0.4), but also from the variation in the pore volume (V_T = 0.039 $cm^3\ g^{-1}$ for Na^+-stevensite and V_T = 0.246 $cm^3\ g^{-1}$ for Ti-stev-0.4), and modification of the pore size distribution upon the formation of the clay mineral by TiO_2 particles. Thereby, the best photocatalytic sample for removal the OG in aqueous solution is Ti-stev-0.4, which implies that the TiO_2 amount used in the preparation of this sample seems to be an optimal value to yield efficient photocatalytic samples. The sample Ti-stev-0.4 is even more active than the TiO_2 powder. In fact, as can be seen in Table 2, the normalized OG conversion values, after 30 min of UV irradiation, are 5.3 and 4.3% of degraded OG/g Ti for, respectively, Ti-stev-0.4 and TiO_2 samples.

CONCLUSIONS

TiO_2/stevensite nanocomposites have been prepared by a solvothermal method by using natural Moroccan Na^+-stevensite as support material. Two nanocomposite photocatalyst referenced as Ti-stev-0.2 and Ti-stev-0.4 were prepared by varying the mass ratio m(TiO_2)/m(Na^+-stevensite), from 0.2:1 and 0.4:1, respectively. Despite the fact that pillaring the stevensite with the TiO_2 particles was not evident in the X-ray diffraction analysis, the Transmission Electronic Microscopy images showed the formation of a TiO_2 matrix in which stevensite and/or pillared stevensite were likely to be embedded.

The sample Ti-stev-0.4 was found to have an important specific surface area and a suitable total pore volume compared with Na^+-stevensite. This nanocomposite exhibits high photocatalytic activity toward the removal of the OG from aqueous solution, and it flocculates very easily, compared with the TiO_2 sample prepared in the absence of Na^+-stevensite. Therefore, this nanocomposite can be recovered from treated waste water without requiring very expensive and sophisticated micro-filtration processes. This study demonstrates the possibility of the valorization of the stevensite of Jbel Rhassoul (Morocco) and it could contribute to the conservation of water by the efficient treatment of waste waters.

ACKNOWLEDGMENTS

Financial support from the "Convention de coopération CNRST-Maroc/CNRS-France" (Chemistry Project No. 04/13) and the "Programme d'Action Intégrée Volubilis" (No. 14/MS/14) is gratefully acknowledged.

REFERENCES

Aït Aghzzaf A., Rhouta B., Steinmetz J., Rocca E., Aranda E., Khalil A., Yvon J. & Daoudi L. (2012) Corrosion inhibitors based on chitosan-heptanoate modified beidellite. *Applied Clay Science*, **65-66**, 173−178.

Aït Aghzzaf A., Rhouta B., Rocca E., Khalil A. & Steinmetz J. (2014) Corrosion inhibition of zinc by calcium-exchanged beidellite clay mineral : a new smart corrosion inhibitor. *Corrosion Science*, **80**, 46−52.

An T., Chen J., Li G., Ding X., Sheng G., Fu J., Mai B. & O'Shea K.E. (2008) Characterization and photocatalytic activity of TiO_2 immobilized hydrophobic montmorillonite photocatalysts: degradation of decabromodiphenyl ether (BDE 209). *Catalysis Today*, **139**, 69−76.

Aranda P., Kun R., Martin Luengo M. A., Letaïef S., Dékány I. & Ruiz-Hitzky E. (2008) Titania-sepiolite nanocomposites prepared by a surfactant templating colloidal route. *Chemistry of Material*, **20**, 84−91.

Benhammou A., Tanouti B., Nibou L., Yaacoubi A. & Bonnet J.P. (2009) Mineralogical and physicochemical investigation of mg-smectite from Jbel Rhassoul, Morocco. *Clays and Clay Minerals*, **57**, 264−270.

Bouna L., Rhouta B., Amjoud M., Jada A., Maury F., Daoudi L. & Senocq F. (2010) Correlation between electrokinetic mobility and ionic dyes adsorption of Moroccan stevensite. *Applied Clay Science*, **48**, 527−530.

Bouna L., Rhouta B., Amjoud M., Maury F., Lafont M.-C., Jada A., Senocq F. & Daoudi L. (2011) Synthesis, characterization and photocatalytic activity of TiO_2 supported natural palygorskite microfibers. *Applied Clay Science*, **52**, 301−311.

Bouna L., Rhouta B., Amjoud M., Maury F., Jada A., Daoudi L., Senocq F., Lafont M.-C. & Drouet C. (2012a) Synthèse, caractérisations et tests photocatalytiques d'un matériau argileux d'origine naturelle à base de beidellite fonctionnalisée par TiO_2. *Matériaux & Techniques*, **100**, 241−252.

Bouna L., Rhouta B., Daoudi L., Maury F., Amjoud M., Senocq F., Lafont M.C., Jada A. & Aîtaghzzaf A. (2012b) Mineralogical and Physico-chemical characterisations of ferruginous beidellite-rich clay from Agadir basin (Morocco). *Clays and Clay Minerals*, **60**, 278−290.

Bouna L., Rhouta B. & Maury F. (2013) Physicochemical study of photocatalytic activity of TiO_2-supported palygorskite clay mineral. *International Journal of Photoenergy*, Article ID 815473, 6 pp. doi:10.1155/2013/815473.

Brunauer S., Emmet P.H. & Teller E. (1938) Adsorption of gases in multimolecular layers. *Journal of American Chemical Society*, **60**, 309−319.

Feng J., Hu X., Yue P. L., Zhu H.-Y. & Lu G. Q. (2003) A novel laponite clay-based Fe nanocomposite and its photo-catalytic activity in photo-assisted degradation of Orange II. *Chemical Engineering Science*, **58**, 679−685.

Frini-Srasra N. & Srasra E. (2010) Acid treatment of south Tunisian palygorskite: Removal of Cd(II) from aqueous and phosphoric acid solutions. *Desalination*, **250**, 26−34.

Hadnadjev Kostic M., Vulic T., Ranogajec J., Marinkovic-Neducin R. & Radosavljevic-Mihajlovic A. (2013) Thermal and photocatalytic behavior of Ti/LDH nanocomposites. *Journal of Thermal Analysis and Calorimetry*, **111**, 1155−1162.

Henych J. & Štengl V. (2013) Feasible Synthesis of TiO_2 Deposited on Kaolin for Photocatalytic Applications. *Clays and Clay Minerals*, **61**, 165−176.

Hofstadler K., Rupert B., Novalic S. & Heisler G. (1994) New reactor design for photocatalytic wastewater treatment with TiO_2 immobilized on fused-silica glass fibers: photomineralization of 4-chlorophenol. *Environmental Science & Technology*, **28**, 670−674.

Holtzapffel T. (1985) Les Minéraux Argileux: Préparation, Analyse Diffractométrique et Détermination. *Société Géologique du Nord Publication*, **12**, 1−136.

Houari M., Saidi, M., Tabet, D., Pichat, P. & Khalaf, H. (2005) The removal of 4-chlorophenol and dichloroacetic acid in water using Ti-, Zr- and Ti/Zr-pillared bentonites as photocatalyst. *American Journal of Applied Sciences*, **2**, 1136−1140.

Jada A., Debih H. & Khodja M. (2006) Montmorillonite surface properties modifications by asphaltenes adsorption. *Journal of Petroleum Science and Engineering*, **52**, 305−316.

Khalfallah Boudali L., Ghorbel A., Tichit D., Chiche B., Dutartre R. & Figueras F. (1994) Synthesis and characterization of titanium-pillared montmorillonites. *Microporous Materials*, **2**, 525−535.

Liu J., Dong M., Zuo S. & Yu Y. (2009) Solvothermal preparation of TiO_2/montmorillonite and photocatalytic activity. *Applied Clay Science*, **43**, 156−159.

Nikolopoulou A., Papoulis D., Komarneni S., Tsolis-Katagas P., Panagiotaras D., Kacandes G.H., Zhang P., Yin S. & Sato T. (2009) Solvothermal preparation of TiO_2/saponite nanocomposites and photocatalytic activity. *Applied Clay Science*, **46**, 363−368.

Ooka C., Yoshida H., Suzuki K. & Hattori T. (2004) Highly hydrophobic TiO_2 pillared clay for photocatalytic degradation of organic compounds in water. *Microporous and Mesoporous Materials*, **67**, 143−150.

Paul B., Martens W.N. & Frost Ray L. (2012) Immobilised anatase on clay mineral particles as a photocatalyst for herbicides degradation. *Applied Clay Science*, **57**, 49−54.

Rhouta B., Kaddami H., Elbarqy J., Amjoud M., Daoudi L., Maury F., Senocq F., Maazouz A. & Gerard J.F. (2008) Elucidating the crystal-chemistry of Jbel Rhassoul stevensite (Morocco) by advanced analytical techniques. *Clay Minerals*, **43**, 393−404.

Rhouta B., Zatile E., Bouna L., Lakbita O., Maury F., Daoudi L., Lafont M.C., Amjoud M., Senocq F., Jada A. & Aït Aghzzaf A. (2013) Comprehensive physicochemical study of dioctahedral palygorskite-rich clay from Marrakech High Atlas (Morocco). *Physics and Chemistry of Minerals*, 40, 411−424.

Seung Mok L. & Diwakar T. (2012) Organo and inorgano-organo-modified clays in the remediation of aqueous solutions: An overview. *Applied Clay Science*, **59–60**, 84−102.